Coupled Seismo-Electromagnetic Interferometry for 2D Homogeneous SH-TE Scenarios

Niels Grobbe, Evert Slob and Kees Wapenaar

Summary
We here explore the application of interferometric principles to the coupled seismo-electromagnetic system. We consider 2D homogeneous space scenarios, and focus on one of the two seismo-electromagnetic propagation modes, the SH-TE mode, where horizontally polarized shear-waves are coupled to the transverse electric mode.

We start by presenting the theory for retrieving seismo-electromagnetic Greenźs function responses via interferometry by cross-correlation.

Using explicit homogeneous space solutions, we numerically investigate the interferometric retrieval of an electric field response and a magnetic field response due to a seismic source. We first study the theoretically desirable circular source configuration, providing illumination from all sides, followed by a more realistic line source configuration, exploiting the interferometric far-field approximation.

These two numerical examples prove for the selected source-receiver type combinations, that we can indeed retrieve correct dynamic seismo-electromagnetic 2D SH-TE responses using seismic boundary sources only. This is a promising result for the next step: applying 3D seismo-electromagnetic interferometry in the field.

Introduction

In porous media, coupled seismo-electromagnetic (seismo-EM) fields of electrokinetic origin can provide seismic resolution, electromagnetic fluid-sensitivity, and reservoir property information like porosity and permeability (Pride, 1994; Revil et al., 2015). One of the key challenges of this geophysical method is the very low signal strength of the coupled signals. One can try to maximize the conversion e.g. using seismo-EM beamforming (Revil et al., 2015), or using brute-force vibroseis trucks (Dean et al., 2012). Having strong sources is not always possible and is likely to boost the noise-levels as well. Therefore, it may be beneficial to replace those sources by receivers: the principle of interferometry. In interferometry, responses recorded at different receivers are cross-correlated to obtain the Green's function between these receivers (Schuster et al., 2004). The cross-correlation process reorganizes measured data, allowing for improved imaging compared to situations where imaging algorithms are applied to the measured data directly. For a 1D scenario for the SH-TE propagation mode (where horizontally polarized shear-waves are coupled to the transverse electric mode), it was shown that correct Green's function retrieval via cross-correlation based interferometry is possible, using only seismic boundary sources (De Ridder et al., 2009; Schoemaker et al., 2012). Eventually, we desire to know the applicability of interferometric principles for seismo-EM field data examples. We here make a first step towards this goal, and present the interferometric theory for 2D scenario's for the SH-TE propagation mode. Using explicit homogeneous space solutions (Grobbe and Slob, 2013), we numerically investigate interferometric retrieval of an electric field and a magnetic field due to a seismic source, for a theoretically desirable circular source configuration, followed by a more realistic line source configuration.

Theory: 2D SH-TE interferometry

We capture the 2D SH-TE system in the general diffusion, flow and wave equation format (following Wapenaar and Fokkema, 2004 (erratum 2010)): $j\omega\mathbf{A}\hat{\mathbf{u}}+\mathbf{B}\hat{\mathbf{u}}+\mathbf{D}_x\hat{\mathbf{u}}=\hat{\mathbf{s}}$. Here, $\hat{\mathbf{u}}$ and $\hat{\mathbf{s}}$ contain the field and source quantities, respectively, whereas $\mathbf{A}$ and $\mathbf{B}$ are matrices containing space-dependent material parameters and $\mathbf{D}_x$ is a matrix containing the spatial differential operators $\frac{\partial}{\partial x_1}$ and $\frac{\partial}{\partial x_3}$. Here, $\hat{\mathbf{u}}^T=\left(\hat{E}_2,\hat{H}_1,\hat{H}_3,\hat{v}_2^s,-\hat{\tau}_{23}^b,-\hat{\tau}_{21}^b\right)$, where $\hat{E}_i$, $\hat{H}_i$, $\hat{v}_i^s$, and $\hat{\tau}_{ij}^b$ are the electric field, the magnetic field, the solid particle velocity, and the bulk stress components, respectively. The subscripts indicate the orientation with respect to the right-handed Cartesian coordinate system and the superscripts provide extra information about the field (or source) type (acting on solid (s), fluid (f), bulk (b) and so on). The superscript T denotes vector or matrix transposition, and the hat symbol indicates the space-frequency domain (or frequency-dependency). The source vector is arranged as $\hat{\mathbf{s}}^T=(\hat{s}_1,\hat{s}_2,\hat{s}_3,\hat{s}_4,\hat{s}_5,\hat{s}_6)$, where $\hat{s}_1=-\hat{J}_2^e-\hat{\mathscr{L}}\hat{f}_2^f$, $\hat{s}_2=-\hat{J}_1^m$, $\hat{s}_3=-\hat{J}_3^m$, $\hat{s}_4=\hat{f}_2^b-\frac{\rho^f}{\hat{\rho}^E}\hat{f}_2^f$, $\hat{s}_5=\hat{h}_{32}^b+\hat{h}_{23}^b$ and $\hat{s}_6=\hat{h}_{12}^b+\hat{h}_{21}^b$. Here, $\hat{h}_{ij}^b$ is the bulk external deformation rate density, where $\hat{h}_{ij}^b=\hat{h}_{ji}^b$, $\hat{J}_i^m$ is the external magnetic current density, $\hat{f}_i^b$ the bulk dipole force source, $\hat{f}_i^f$ the fluid dipole force source, and $\hat{J}_i^e$ the external electric current density. Furthermore, ρ^f is the density of the pore-fluid, $\hat{\mathscr{L}}$ the seismo-EM coupling coefficient, and $\hat{\rho}^E=\frac{\eta}{s\hat{k}}$, where η is the viscosity of the fluid, $\hat{k}$ the permeability of the medium, and $s=j\omega$ (with ω being the radial frequency and j denoting the imaginary unit). For the details of $\mathbf{A}$, $\mathbf{B}$ and $\mathbf{D}_x$, the reader is referred to Wapenaar and Fokkema, 2004 (erratum 2010). By replacing the source vector $\hat{\mathbf{s}}$ by a point source matrix $\mathbf{I}\delta(\mathbf{x}-\mathbf{x}_A)$, the field quantities in $\hat{\mathbf{u}}$ can be replaced by a Green's matrix, resulting in

$$\hat{\mathbf{G}}(\mathbf{x}_B,\mathbf{x}_A,\omega)=\begin{pmatrix}\hat{G}^{E_2,s_1} & \hat{G}^{E_2,s_2} & \hat{G}^{E_2,s_3} & \hat{G}^{E_2,s_4} & \hat{G}^{E_2,s_5} & \hat{G}^{E_2,s_6}\\ \hat{G}^{H_1,s_1} & \hat{G}^{H_1,s_2} & \hat{G}^{H_1,s_3} & \hat{G}^{H_1,s_4} & \hat{G}^{H_1,s_5} & \hat{G}^{H_1,s_6}\\ \hat{G}^{H_3,s_1} & \hat{G}^{H_3,s_2} & \hat{G}^{H_3,s_3} & \hat{G}^{H_3,s_4} & \hat{G}^{H_3,s_5} & \hat{G}^{H_3,s_6}\\ \hat{G}^{v_2,s_1} & \hat{G}^{v_2,s_2} & \hat{G}^{v_2,s_3} & \hat{G}^{v_2,s_4} & \hat{G}^{v_2,s_5} & \hat{G}^{v_2,s_6}\\ \hat{G}^{\tau_{23},s_1} & \hat{G}^{\tau_{23},s_2} & \hat{G}^{\tau_{23},s_3} & \hat{G}^{\tau_{23},s_4} & \hat{G}^{\tau_{23},s_5} & \hat{G}^{\tau_{23},s_6}\\ \hat{G}^{\tau_{21},s_1} & \hat{G}^{\tau_{21},s_2} & \hat{G}^{\tau_{21},s_3} & \hat{G}^{\tau_{21},s_4} & \hat{G}^{\tau_{21},s_5} & \hat{G}^{\tau_{21},s_6}\end{pmatrix}, \tag{1}$$

where $\mathbf{x}_A$ corresponds to the source location and $\mathbf{x}_B$ to the receiver location and the superscripts denote (receiver-type, source-type), according to their position in $\hat{\mathbf{u}}$ and $\hat{\mathbf{s}}$, respectively. Each of the elements corresponds to a Green's function which we can model using the homogeneous space Green's function expressions (Grobbe and Slob, 2013). We can now select the Green's function for a certain seismo-EM

source-receiver combination and evaluate the interferometric Green's function retrieval expression as presented in Wapenaar et al. (2006):

$$\hat{\mathbf{G}}(\mathbf{x}_B,\mathbf{x}_A,\omega)+\hat{\mathbf{G}}^{\dagger}(\mathbf{x}_A,\mathbf{x}_B,\omega) = -\oint_{\partial S}\hat{\mathbf{G}}(\mathbf{x}_B,\mathbf{x},\omega)\mathbf{N}_x\hat{\mathbf{G}}^{\dagger}(\mathbf{x}_A,\mathbf{x},\omega)d\mathbf{x}+ \int_S\hat{\mathbf{G}}(\mathbf{x}_B,\mathbf{x},\omega)\left(j\omega 2j\Im(\hat{\mathbf{A}})+\hat{\mathbf{B}}+\hat{\mathbf{B}}^{\dagger}\right)\hat{\mathbf{G}}^{\dagger}(\mathbf{x}_A,\mathbf{x},\omega), \quad (2)$$

where the first term on the left-hand side represents the causal retrieved Green's function with the virtual source at receiver location $\mathbf{x}_A$ and the receiver at $\mathbf{x}_B$ and where the second term represents the acausal retrieved Green's function with the virtual source at receiver location $\mathbf{x}_B$ and the receiver at $\mathbf{x}_A$. The dagger sign denotes the complex conjugate transpose. Furthermore, the first integral on the right-hand side is the boundary source integral, summing the contributions from different source locations $\mathbf{x}$ to receivers $\mathbf{x}_A$ and $\mathbf{x}_B$ and the second integral represents the volume source integral. $\mathbf{N}_x$ is the matrix consisting of normal vector elements n_1 and n_3 with positions and signs equal to the organization of partial derivative matrix $\mathbf{D}_x$. We here focus on element (1,4) of equation 1, and evaluate expression 2 for this element considering only boundary source contributions, which results in

$$\left[\hat{G}^{E_2,s_4}(\mathbf{x}_B,\mathbf{x}_A,\omega)+\left\{\hat{G}^{v_2,s_1}(\mathbf{x}_A,\mathbf{x}_B,\omega)\right\}^*\right]\hat{S} = -\oint_{\partial S}\Big[\hat{G}_B^{E_2,s_1}(-n_3)(\hat{G}_A^{v_2,s_2})^* + \hat{G}_B^{E_2,s_1}n_1(\hat{G}_A^{v_2,s_3})^* + \hat{G}_B^{E_2,s_2}(-n_3)(\hat{G}_A^{v_2,s_1})^* + \hat{G}_B^{E_2,s_3}n_1(\hat{G}_A^{v_2,s_1})^* + \hat{G}_B^{E_2,s_4}n_3(\hat{G}_A^{v_2,s_5})^* + \hat{G}_B^{E_2,s_4}n_1(\hat{G}_A^{v_2,s_6})^* + \hat{G}_B^{E_2,s_5}n_3(\hat{G}_A^{v_2,s_4})^* + \hat{G}_B^{E_2,s_6}n_1(\hat{G}_A^{v_2,s_4})^*\Big]\hat{S}d\mathbf{x}, \quad (3)$$

where the subscript B replaces the spatial and frequency terms in the Green's function argument $(\mathbf{x}_B,\mathbf{x},\omega)$ and where the subscript A replaces $(\mathbf{x}_A,\mathbf{x},\omega)$. We model all Green's functions using a Ricker wavelet with a peak frequency of 30 Hz. In the above equation, $\hat{S}$ denotes the power spectrum of this Ricker wavelet and the asterix denotes complex conjugation. We model the left-hand side of equation 3 as the reference response (displayed in blue-solid), whereas the right-hand side results in the interferometrically retrieved response (displayed in red-dashed). Similar integral representations can be derived and modeled for all other seismo-EM source-receiver combinations (including the combination of our second numerical example).

Numerical Results: Circular Source and Line Source Configurations

Our aim is to investigate whether we can retrieve correct seismo-EM responses using correlation-based interferometry with boundary sources only, preferably of a certain type. We first consider a 2D circular source geometry in the (x_1,x_3)-plane with two receivers located at $\mathbf{x}_A=(0,-200)$ and $\mathbf{x}_B=(0,200)$ and 500 sources located at the boundary of the circle with centerpoint $=(0,0)$ and radius R=1200 m. Having illumination from all sides, we should theoretically be able to retrieve the response matching in both phase and amplitude. However, the volume source terms in equation 2 account for the losses. When losses occur, using only boundary sources might not yield the desired retrieved responses. We consider a porous, fluid-saturated medium with properties such that in the frequency bandwidth under consideration (0-500 Hz) the S-wave velocity range is $\hat{c}_{SH}=2110.8-2110.9$ m/s and the transverse electric field diffusive velocity range is $\hat{c}_{TE}=31421.5-1005811.5$ m/s. Since we model a homogeneous medium, only coseismic fields (EM fields copropagating within seismic waves) and source-converted fields (conversion to EM at the source impact) are to be expected, and no interface response fields (independent EM fields generated at interfaces from seismic incoming waves). We use explicit homogeneous space Green's function expressions (Grobbe and Slob, 2013) to model the responses. We investigate the retrieval of two source-receiver combinations, $G^{E_2,s_4}(\mathbf{x}_B,\mathbf{x}_A,t)+G^{v_2,s_1}(\mathbf{x}_A,\mathbf{x}_B,-t)$ and $G^{H_1,s_4}(\mathbf{x}_B,\mathbf{x}_A,t)+G^{v_2,s_2}(\mathbf{x}_A,\mathbf{x}_B,-t)$, where the positive times represent the causal responses and the time-reversals the acausal responses. The distance between receivers $\mathbf{x}_A$ and $\mathbf{x}_B$ is 400 m, resulting in a direct coseismic event at a S-wave arrival time of around t=0.19 s. Furthermore, we expect a source-converted field with EM velocity, arriving more or less instantaneously at t=0. The results of these two interferometric numerical experiments are displayed in Figures 1a and 1b, respectively. We observe that by using all boundary source-types, we correctly retrieve the desired direct S-wave event in the causal part in both phase and amplitude, for both source-receiver combinations. The acausal parts of Figure 1

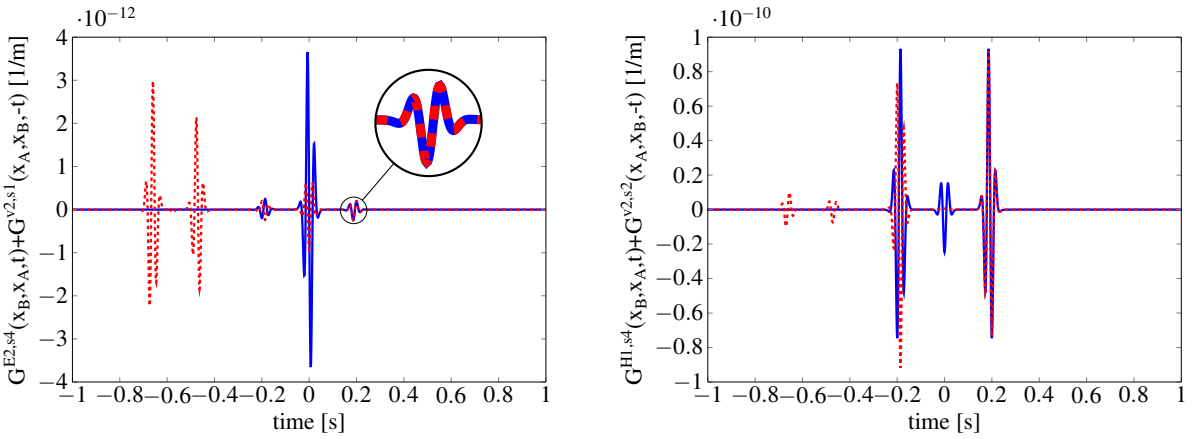

(a) (b)

Figure 1 *Interferometric retrieval using all boundary source-types for a circular acquisition geometry. Blue: reference, red-dashed: retrieved.* **(a)** *Interferometric retrieval of* $G^{E_2,s_4}(\mathbf{x}_B,\mathbf{x}_A,t)+G^{v_2,s_1}(\mathbf{x}_A,\mathbf{x}_B,-t)$ **(b)** *Interferometric retrieval of* $G^{H_1,s_4}(\mathbf{x}_B,\mathbf{x}_A,t)+G^{v_2,s_2}(\mathbf{x}_A,\mathbf{x}_B,-t)$.

display a polarity reversed direct arrival and two additional spurious events. The instantaneously converted EM arrival at t=0 s is not correctly retrieved using boundary sources only. The boundary sources only slightly contribute to this source-converted EM field in Figure 1a, and hardly in Figure 1b. Based on our knowledge from 1D results (De Ridder et al., 2009; Schoemaker et al., 2012), we expect that by adding the volume source contributions, the spurious events will vanish, the polarity of the acausal direct S-wave arrival will be reversed and the instantaneous converted EM arrival will be retrieved correctly. The volume sources are not required for retrieving the events in the causal part. Since we are interested in the causal part of the response, the losses in the medium do not matter.

We now move on to a scenario where sources located at two horizontal lines above and below the receiver levels. We use two source arrays located at -1200 m and 1200 m depth, both containing 1025 sources with 4 m source spacing. We apply a far-field approximation, meaning that only the terms in equation 3 related to the n_3 normal components are contributing. A Hanning taper with a taper length of 500 is applied, tapering the non-stationary zones to avoid artefacts. The receivers are located at the same positions as before, and we investigate the same Green's function retrieval. Figures 2a and d show again a perfect dynamic retrieval of the causal direct shear-wave related coseismic field. Comparing the red-dashed retrieved signal of Figure 2a, with the circular source configuration of Figure 1a, the amplitudes of the acausal spurious events are now slightly less, and also the source-converted field contribution is of smaller amplitude. Figures 2b and e show the retrieved response using only seismic boundary sources. For both scenarios, we still observe perfect retrieval of the event in the causal part without visible amplitude losses. There is no visible contribution of the seismic boundary sources to the source-converted EM field. Figures 2c and f present the retrieved events using only EM boundary sources. In Figure 2c, we can indeed observe that these sources do not contribute to the retrieval of the S-wave velocity related direct coseismic fields, but they do contribute to the instantaneously source-converted EM field at t=0 and to the spurious events at negative times greater than t=-0.25 s. Figure 2f emphasizes that the EM boundary sources do not visibly contribute to the source-converted EM field for the magnetic field recovery, and that this field will be almost completely recovered by the volume sources accounting for the losses in the medium.

Conclusions

The theory for interferometric retrieval of 2D SH-TE seismo-EM Green's functions was presented. Using both a circular source configuration and a line source configuration, we have shown that we can correctly retrieve the dynamic seismo-EM 2D SH-TE response, using seismic boundary sources only. This was demonstrated for two source-receiver combinations: an electric field and a magnetic field due to a seismic source. The volume source contributions account for the losses in the acausal part of the

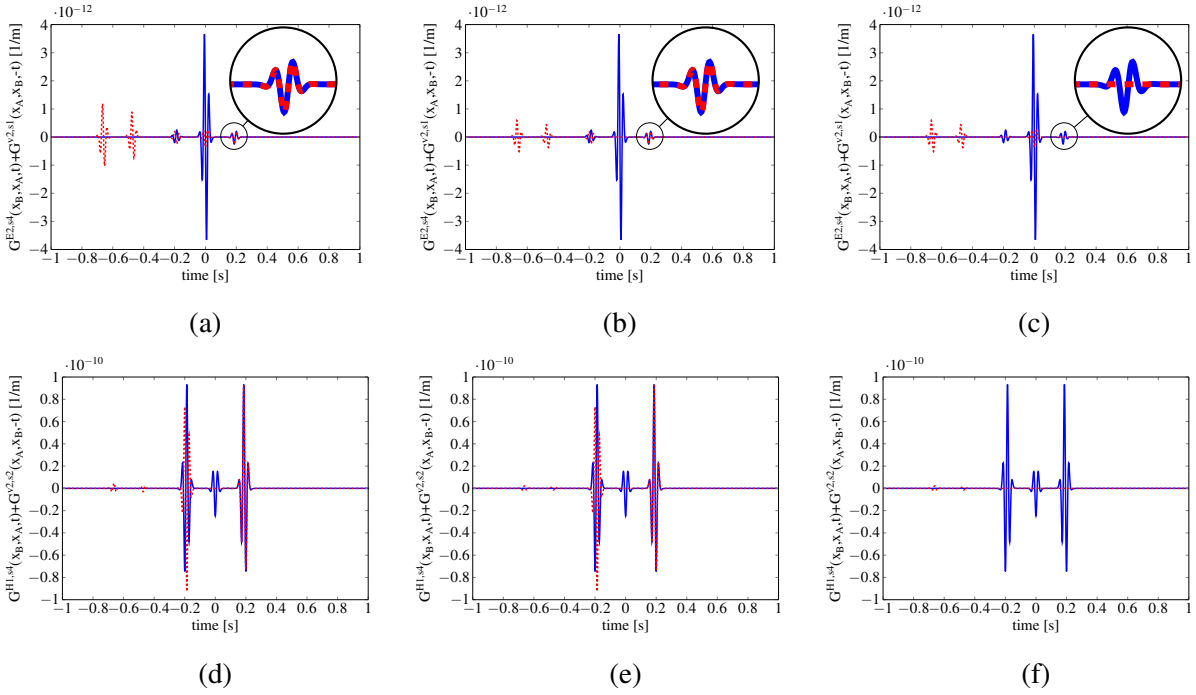

Figure 2 *Interferometric retrieval of (top)* $G^{E_2,s_4}(\mathbf{x}_B,\mathbf{x}_A,t)+G^{v_2,s_1}(\mathbf{x}_A,\mathbf{x}_B,-t)$*, and (bottom)* $G^{H_1,s_4}(\mathbf{x}_B,\mathbf{x}_A,t)+G^{v_2,s_2}(\mathbf{x}_A,\mathbf{x}_B,-t)$ *using:* **(a,d)** *All boundary source-types* **(b,e)** *Seismic boundary sources only* **(c,f)** *EM boundary sources only. Blue: reference, red-dashed: retrieved.*

retrieved response as well as the instantaneous source-converted EM field.

Acknowledgements

The research was funded as a Shell Global Solutions International B.V.-FOM project within the research program "Innovative physics for oil and gas". The authors are grateful to Rik Noorlandt and Jürg Hunziker for stimulating discussions.

References

De Ridder, S., Slob, E. and Wapenaar, K. [2009] Interferometric seismoelectric Green's function representations. *Geophysical Journal International*, **178**, 1289–1304.

Dean, T., Dupuis, J., Herrmann, R. and Valuri, J. [2012] A brute-strength approach to improving the quality of seismoelectric data. *SEG Annual Meeting Las Vegas*, 1–5.

Grobbe, N. and Slob, E. [2013] Validation of an electroseismic and seismoelectric modeling code, for layered earth models, by the explicit homogeneous space solutions. *SEG Annual Meeting Houston*, 1847–1851.

Pride, S. [1994] Governing equations for the coupled electromagnetics and acoustics of porous media. *Physical Review B.*, **50**.

Revil, A., Jardani, A., Sava, P. and Haas, A. [2015] *The Seismoelectric Method: Theory and Application*. John Wiley & Sons.

Schoemaker, F., Grobbe, N., Schakel, M., de Ridder, S., Slob, E. and Smeulders, D. [2012] Experimental Validation of the Electrokinetic Theory and Development of Seismoelectric Interferometry by Cross-Correlation. *International Journal of Geophysics*, **2012**.

Schuster, G., Yu, J., Sheng, J. and Rickett, J. [2004] Interferometric/daylight seismic imaging. *Geophysical Journal International*, **157**, 838–852.

Wapenaar, K. and Fokkema, J. [2004 (erratum 2010)] Reciprocity theorems for diffusion, flow and waves. *Journal of Applied Mechanics*, **71**, 145–150.

Wapenaar, K., Slob, E. and Snieder, R. [2006] Unified Green's Function Retrieval by Cross Correlation. *Physical Review Letters*, **97**, 234301–1 – 234301–4.